ACS APPLIED MATERIALS & INTERFACES

Research Article

www.acsami.org

Combining the UV-Switchability of Keggin Ions with a Galvanic Replacement Process to Fabricate TiO_2–Polyoxometalate–Bimetal Nanocomposites for Improved Surface Enhanced Raman Scattering and Solar Light Photocatalysis

Andrew Pearson,[†] Sheshanath Bhosale,[‡] Suresh K. Bhargava,[‡] and Vipul Bansal*[,†,‡]

[†]NanoBiotechnology Research Lab (NBRL) and [‡]Centre for Advanced Materials & Industrial Chemistry, RMIT University, GPO Box 2476 V, Melbourne VIC 3001, Australia

Supporting Information

ABSTRACT: While the decoration of TiO_2 surfaces with metal nanoparticles has been well-established, the modification of the composition of metal nanoparticles postdeposition onto TiO_2 surfaces and applicability of such bimetallic systems for surface enhanced Raman scattering (SERS) and photocatalysis has not hitherto been investigated. In this work, we, for the first time, combine the unique UV-switchability of the Keggin ions of 12-phosphotungstic acid (PTA) to directly form metal nanoparticles (Ag and Cu) onto the colloidal TiO_2 surface, with a galvanic replacement process to convert these predeposited metal nanoparticles into bimetallic systems (Ag/Au, Ag/Pt, Cu/Au, Cu/Pt, and Cu/Ag). We further demonstrate the applicability of these novel TiO_2–polyoxometalate–bimetal nanocomposites toward improved SERS and solar light photocatalysis.

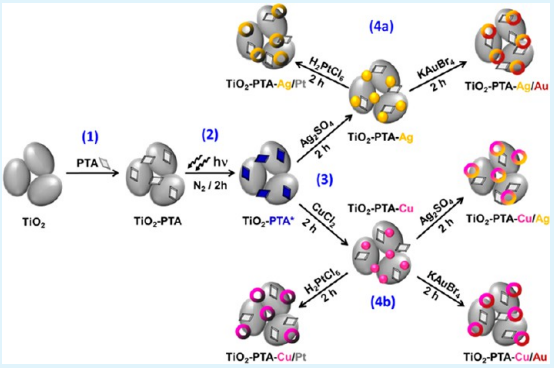

KEYWORDS: *TiO_2, Keggin ions, bimetallic nanoparticles, SERS, photocatalysis*

1. INTRODUCTION

It has been long established that titania (TiO_2) is an excellent candidate for a broad range of applications due to its intriguing physicochemical properties as a wide band gap semiconductor that offers desirable features including low-cost, abundance, and a relatively nontoxic nature. In many cases, TiO_2 has been demonstrated to enhance the catalytic activity of a system due to strong interactions between the active phase and the TiO_2 support,[1,2] wherein, in particular, the anatase phase of TiO_2 enjoys tremendous attention for potential applications in paints and the photodegradation of environmentally toxic dyes[3,4] and organic pollutants.[5,6] However, the major problem associated with the application of TiO_2 particles is the phenomenon known as charge recombination (or electron–hole recombination) whereby an inherently large driving force promotes the recombination of the electron and the newly generated hole upon photoexcitation that reduces its overall photocatalytic performance.[7] Additionally, a rather large band gap of TiO_2 (3.2 eV)[8] means that this material typically requires exposure to ultraviolet (UV) radiation to promote electrons to the conduction band for photocatalysis applications, which is neither energy-efficient, nor easily applicable for household applications.

As such, a great deal of effort has been put forward to shift the band gap energy of TiO_2 particles toward the visible region of the spectrum[8−11] where photoexcitation can become more energetically favorable. In addition to shifting the band gap, significant efforts have been directed to introduce small amounts of transition metals into the TiO_2 matrix, which is observed to suppress the electron–hole recombination to some extent.[12,13] Previously, both chemical and photodeposition techniques have been employed to facilitate the deposition of noble metal particles onto the surface of semiconductor TiO_2, whereby the introduction of metal nanoparticles has been demonstrated to enhance the photocatalytic activity of the system.[14−16] Unfortunately, many synthetic pathways such as the self-assembled monolayer approach,[17−20] RF-sputtering,[12,21] liquid phase deposition,[22] impregnation, and ion exchange[23] often require adverse conditions such as high temperatures and pressures to be viable, and these synthesis procedures typically result in a mixture containing metal-decorated TiO_2 particles and free metal nanoparticles.

Recently, we demonstrated that polyoxometalates (POMs—a class of heteropolyacids, which are themselves photocatalytic) can be utilized as highly efficient photoactive linker molecules to facilitate the deposition of noble metal nanoparticles directly on the surface of TiO_2 particles without causing nucleation of standalone free metal nanoparticles in the solution.[24−26] We found that the employment of POMs of Keggin ion structure is highly advantageous for this purpose as they generally possess

Received: April 7, 2013
Accepted: July 15, 2013
Published: July 15, 2013

Scheme 1. Representation of the Formation of TiO_2–PTA–Bimetal Nanocomposite Materials[a]

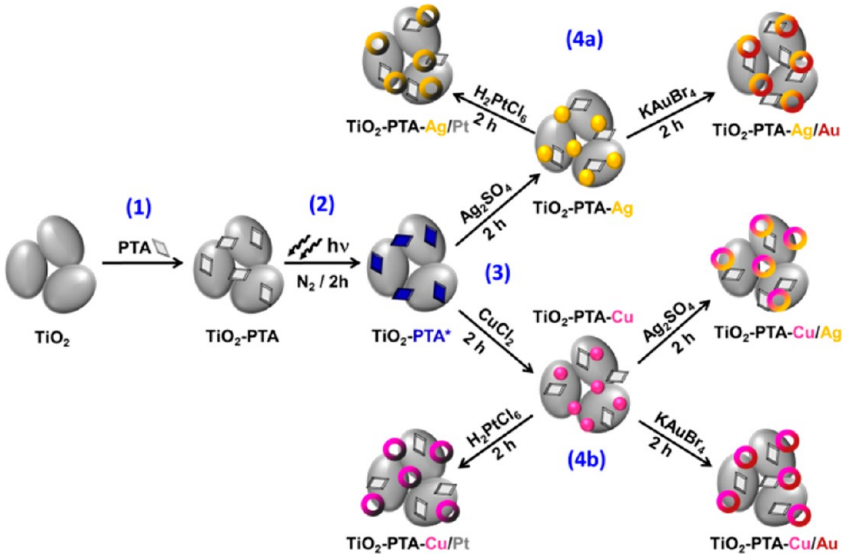

[a]The colors have been used as a guide to depict the bimetallicity of the resultant nanoshells.

very high thermal stability[27] and can undergo stepwise multielectron redox processes without undergoing structural changes.[28] Importantly, POM molecules bound to the surface of TiO_2 particles can themselves act as a highly localized, UV-switchable reducing agent for metal ions to controllably deposit metal nanoparticles on the TiO_2 surface. Notably, our previous work was inspired from a pioneering work demonstrating that exposure of a photoreduced POM (silicotungstic acid $[(SiW_{12}O_{40})^{4-}]$) to metal ions may result in stable metal nanoparticles capped with Keggin ions,[29] which has been explored to prepare a variety of interesting nanomaterials.[28,30] Interestingly, while the decoration of noble metal nanoparticles on the surface of TiO_2 particles has been achieved by several groups, including our recent work on utilization of POMs to achieve metal nanoparticle contaminant-free synthesis of TiO_2–POM–metal,[24−26] the postsynthesis modification of TiO_2–metal composites to obtain a bimetallic nanocomposite remains to be investigated.

During the past decade, the galvanic replacement approach has been enthusiastically investigated as a facile electroless approach to prepare bimetallic nanomaterials of unique architectures.[31−37] In the current study, we, for the first time, combine the unique ability of POMs to prepare metal nanoparticle-free TiO_2–POM–metal nanocomposites with that of galvanic replacement process to convert a monometallic system into bimetallic. These new TiO_2–POM–bimetallic systems offer the next level of control over properties and applicability of monometallic systems previously reported by our group. Specifically, we herein report for the first time the galvanic replacement of metal nanoparticles of silver (AgNP) and copper (CuNP) deposited onto TiO_2 particles, to form different compositions of TiO_2-supported bimetallic (Ag/Au, Ag/Pt, Cu/Au, Cu/Pt, and Cu/Ag) nanoparticles. 12-Phosphotungstic acid (PTA) is one of the strongest heteropolyacids, and we utilize PTA as the model POM Keggin ion in this study. The applications of these novel TiO_2–PTA–bimetallic materials toward surface enhanced Raman spectroscopy (SERS) sensing of rhodamine-6B and the photocatalytic degradation of the organic azo dye Congo red under simulated solar light conditions have been explored.

2. EXPERIMENTAL SECTION

2.1. Materials. Potassium tetrabromoaurate ($KAuBr_4·3H_2O$), chloroplatinic acid ($H_2PtCl_6·2H_2O$), cupric chloride ($CuCl_2$), and silver sulfate (Ag_2SO_4) were obtained from Sigma Aldrich; anatase titanium dioxide powder and propan-2-ol (isopropanol) were obtained from BDH Chemicals, and 12-phosphotungstic acid hydrate (PTA–$H_3PW_{12}O_{40}·3H_2O$) was obtained from Scharlau Chemie. All chemicals were used as received.

2.2. PTA Functionalization of TiO_2 Nanoparticles. To a 10 mL aqueous solution containing 10 mM PTA, 100 mg of anatase TiO_2 powder was added and allowed to surface-functionalize overnight under mechanical stirring to prevent the powder from settling. After 24 h, the composite was centrifuged at 3000 rpm to facilitate the removal of unbound PTA molecules, the supernatant was removed, and the solid material was washed thrice with deionized Milli-Q water. The composite was redispersed in 25 mL of deionized water and is designated as TiO_2–PTA.

2.3. Decoration of TiO_2–PTA Composite with Silver and Copper Nanoparticles. To decorate the TiO_2–PTA composite with silver and copper nanoparticles, the ability of PTA to act as a UV-switchable reducing agent was exploited. In two parallel experiments, 1 mL isopropanol was added to 4 mL of the TiO_2–PTA composite in a quartz tube and subsequently purged with N_2 gas for 15 min. The solutions were then photoexcited using UV lamp (excitation wavelength of 253 nm) for a period of 2 h to facilitate the reduction of the TiO_2 bound PTA molecules. A 5 mL portion of aqueous 1 mM Ag_2SO_4 or $CuCl_2$ was added to the respective quartz tubes containing the reduced state of TiO_2–PTA* and allowed to mature for 2 h, following which, the products were centrifuged at 3000 rpm, washed thrice with deionized water, and suspended in 25 mL of deionized water. The TiO_2–PTA–Ag composite was light yellow/brown in color while the TiO_2–PTA–Cu composite was initially of very light pink color.

2.4. Galvanic Replacement of TiO_2–PTA–Metal Composites with Silver, Gold, and Platinum Ions. Galvanic replacement reactions were performed by immersing TiO_2–PTA–Ag and TiO_2–PTA–Cu composites independently in solutions containing a suitable metal ion. To two separate solutions containing 2 mL of the TiO_2–PTA–Ag composite, 6 mL of aqueous $KAuBr_4$ (0.1 mM), and 4 mL of aqueous H_2PtCl_6 (0.1 mM) were added, and the final volume was made up to 10 mL with deionized water. After mixing, the solutions were observed to rapidly change colors from light yellow/brown to a light violet in the case of $KAuBr_4$ addition and to a dark gray in the case of H_2PtCl_6 addition. These reaction products are designated as

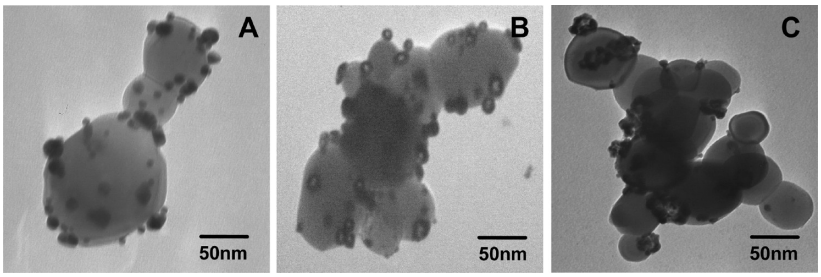

Figure 1. TEM images of (A) TiO_2–PTA–Ag, (B) TiO_2–PTA–Ag/Pt, and (C) TiO_2–PTA–Ag/Au nanocomposites.

TiO_2–PTA–Ag/Au and TiO_2–PTA–Ag/Pt for silver galvanically replaced with gold and platinum, respectively. Concurrently, to three solutions, each containing 2 mL of the TiO_2–PTA–Cu composite, 4 mL of aqueous Ag_2SO_4 (0.1 mM), 3 mL of aqueous $KAuBr_4$ (0.1 mM), and 2 mL of aqueous H_2PtCl_6 (0.1 mM) were separately added, and the final volume was adjusted to 10 mL with deionized water. The solutions were observed to change color after approximately 15 min from pinkish–white to a light gray for Ag_2SO_4 addition, light violet for $KAuBr_4$ addition, and dark gray for H_2PtCl_6 addition. The galvanic replacement reactions were allowed to proceed overnight to ensure that the reactions went to completion. These reaction products are designated as TiO_2–PTA–Cu/Ag, TiO_2–PTA–Cu/Au, and TiO_2–PTA–Cu/Pt for copper galvanically replaced with silver, gold, and platinum, respectively. As the amount of metal deposited from a galvanic replacement reaction is dependent on the oxidation states of the reactants, different amounts of metal ions were added in an attempt to ensure that similar amounts of copper (in the case of TiO_2–PTA–Cu) and silver (in the case of TiO_2–PTA–Ag) are consumed during the galvanic replacement process.

2.5. Photocatalysis, SERS Studies, and Instrumentation. The photocatalytic activity of the prepared TiO_2-based nanocomposites was studied by immersing 12 mg equivalent of TiO_2 in 10 mL of an aqueous solution containing 10 μM Congo red (CR). The activity was recorded by computing the intensity of the characteristic absorption maxima (λ_{max} 500 nm) after a period of 30 min exposure to simulated solar light. An Abet Technologies LS-150 Series 150W Xe Arc Lamp Source which simulated the solar spectrum at equatorial conditions was used with the sample placed in a quartz vial 10 cm from the source aperture, under mechanical stirring. After irradiation for 30 min, samples were centrifuged to remove the nanocomposites, and the remaining solutions were examined by UV–vis spectroscopy. Surface enhanced Raman scattering (SERS) studies were performed on a Perkin-Elmer RamanStation 400F using rhodamine-6B as a probe molecule. SERS substrates were prepared by drop casting 20 μL of nanocomposite on a Si (100) substrate followed by solvent evaporation. For SERS analysis, 10 μL of aqueous 10 μM rhodamine-6B solution was drop cast on to SERS substrates and the solvent allowed to evaporate before SERS analysis being performed using Raman focus and 100% laser power. Transmission electron microscopy (TEM) was performed on a Jeol 1010 TEM operating at 100 kV, and samples for TEM were prepared by drop casting 10 μL of respective material onto a 200 mesh copper grid with strong carbon film and allowing the solvent to evaporate.

3. RESULTS AND DISCUSSION

3.1. Nanocomposite Synthesis, Galvanic Replacement Reactions, and Materials Characterization. Illustrated in Scheme 1 is a simplified series of reactions that were employed for the synthesis of TiO_2–PTA–bimetal nanocomposites. First, in step 1, Degussa P25 anatase TiO_2 particles are functionalized with PTA molecules ($[PW_{12}O_{40}]^{3-}$), which results in TiO_2–PTA particles. Step 2 involves exposing the TiO_2–PTA particles to UV irradiation for 2 h in the presence of propan-2-ol in an N_2 environment. Since PTA is a UV-switchable reducing agent, step 2 leads to the reduction of $[PW_{12}O_{40}]^{3-}$ ions bound to the TiO_2 surface to $[PW_{12}O_{40}]^{4-}$ ions (represented as the blue colored PTA*). This reduction of PTA molecules upon UV irradiation results in the particle color change from milky white to purplish blue, characteristic of the reduced state of PTA.[28] In step 3, the reduced TiO_2–PTA* composite is independently exposed to suitable metal salts containing Ag^+ or Cu^{2+} ions for 2 h, during which the reduced PTA* bound to the TiO_2 surface acts as a highly localized reducing agent to convert metal ions into AgNPs or CuNPs, respectively, directly onto the surface of the TiO_2 particles. This results in a change in the solution color from purplish–blue to brown–yellow for decoration with AgNPs (TiO_2–PTA–Ag) and light pink for decoration with CuNPs (TiO_2–PTA–Cu). At this point, step 4 is split into two parts: step 4a depicts the galvanic replacement of the Ag nanoparticles with $[PtCl_6]^{2-}$ and $[AuBr_4]^-$ ions, wherein TiO_2–PTA–Ag composite was separately immersed in solutions containing these ions and allowed to react overnight to ensure the galvanic replacement reaction reached conclusion. Within 15 min, the color of the galvanically replaced nanocomposites changed from brown–yellow to dark gray for $[PtCl_6]^{2-}$ addition and light violet for $[AuBr_4]^-$ addition. Step 4b shows a similar process whereby CuNPs deposited on the TiO_2 surface in the TiO_2–PTA–Cu nanocomposite are galvanically replaced with Ag^+, $[PtCl_6]^{2-}$, and $[AuBr_4]^-$ ions, resulting in change in nanocomposites color from light pink to light gray for Ag^+ addition, dark gray for $[PtCl_6]^{2-}$ addition, and light violet for $[AuBr_4]^-$ addition.

The galvanic replacement reactions described above in step 4a can be described by eqs 1 and 2 for galvanic replacement of AgNPs with $[PtCl_6]^{2-}$ and $[AuBr_4]^-$ ions, respectively,

$$4Ag_{(s)}^{\ 0} + [PtCl_6]_{(aq)}^{\ 2-} \rightarrow 4Ag_{(aq)}^{\ +} + Pt_{(s)}^{\ 0} + 6Cl_{(aq)}^{\ -} \quad (1)$$

$$3Ag_{(s)}^{\ 0} + [AuBr_4]_{(aq)}^{\ -} \rightarrow 3Ag_{(aq)}^{\ +} + Au_{(s)}^{\ 0} + 4Br_{(aq)}^{\ -} \quad (2)$$

and by eqs 3–5 for galvanic replacement of CuNPs with Ag^+, $[PtCl_6]^{2-}$, and $[AuBr_4]^-$ ions (step 4b), respectively:

$$Cu_{(s)}^{\ 0} + 2Ag_{(aq)}^{\ +} \rightarrow Cu_{(aq)}^{\ 2+} + 2Ag_{(s)}^{\ 0} \quad (3)$$

$$2Cu_{(s)}^{\ 0} + [PtCl_6]_{(aq)}^{\ 2-} \rightarrow 2Cu_{(aq)}^{\ 2+} + Pt_{(s)}^{\ 0} + 6Cl_{(aq)}^{\ -} \quad (4)$$

$$3Cu_{(s)}^{\ 0} + 2[AuBr_4]_{(aq)}^{\ -} \rightarrow 3Cu_{(aq)}^{\ 2+} + 2Au_{(s)}^{\ 0} + 8Br_{(aq)}^{\ -} \quad (5)$$

It is noteworthy that galvanic replacement engaging AgNPs and CuNPs can, in principle, be pursued to any metal ions whose redox potential is higher than that of Ag^+/Ag pair (~0.80 V vs standard hydrogen electrode (SHE)) and Cu^{2+}/Cu

pair (0.34 V vs SHE), respectively. The redox potential of the $AuBr_4^-$/Au pair (0.85 V vs SHE) and the Pt^{4+}/ Pt pair (~0.86 V vs SHE) are higher than those both of Ag^+/Ag and Cu^{2+}/Cu pairs; therefore, these reactions could be pursued in both the cases. Similarly since the redox potential of the Ag^+/Ag pair is higher than that of Cu^{2+}/Cu pair, an additional reaction could be examined in the case of CuNPs.

TEM images depicting the galvanic replacement of TiO_2–PTA–Ag nanocomposite with $[PtCl_6]^{2-}$ and $[AuBr_4]^-$ ions are displayed in Figure 1. Figure 1A shows the TiO_2–PTA–Ag composite before galvanic replacement, wherein the irregularly shaped commercial anatase TiO_2 particles vary in diameter from 50 to 200 nm, further decorated with ca. 10–20 nm quasi-spherical Ag NPs using a PTA-mediated photoreduction approach can be observed. Galvanic replacement of TiO_2–PTA–Ag with $[PtCl_6]^{2-}$ ions results in TiO_2–PTA–Ag/Pt nanocomposite (Figure 1B), wherein the AgNPs on the TiO_2 surface undergo a morphology change resulting in hollow Ag/Pt bimetallic nanoshells. Since it is well-established that galvanic replacement reactions in aqueous solutions typically undergo a pinhole forming mechanism, leading to hollow nanoarchitectures, observation of similar hollow structures in this study indicates the involvement of a galvanic replacement process to form bimetallic alloys in our study.[32] Similarly, when TiO_2–PTA–Ag composite was exposed to $[AuBr_4]^-$ ions; TiO_2–PTA–Ag/Au consisting of hollow Ag/Au particles were obtained (Figure 1C). The additional low magnification TEM images of TiO_2–PTA–Ag based nanocomposites are shown in the Supporting Information (Figure S1).

Galvanic replacement reaction of TiO_2–PTA–Cu nanocomposites with Ag^+, $[PtCl_6]^{2-}$, and $[AuBr_4]^-$ ions (Figure 2) produced similar outcomes as that of TiO_2–PTA–Ag nanocomposite (Figure 1). Pristine TiO_2–PTA–Cu nanocomposite (Figure 2A) showed ca. 10–20 nm quasi-spherical CuNPs decorating the surface of the irregularly shaped 50–200 nm TiO_2 particles, which after reaction with different metal ions, underwent a morphology change to form respective hollow bimetals, leading to TiO_2–PTA–Cu/Ag (Figure 2B), TiO_2–PTA–Cu/Pt (Figure 2C), and TiO_2–PTA–Cu/Au (Figure 2D) nanocomposites. The additional low magnification TEM images of TiO_2–PTA–Cu based nanocomposites are shown in the Supporting Information (Figure S2).

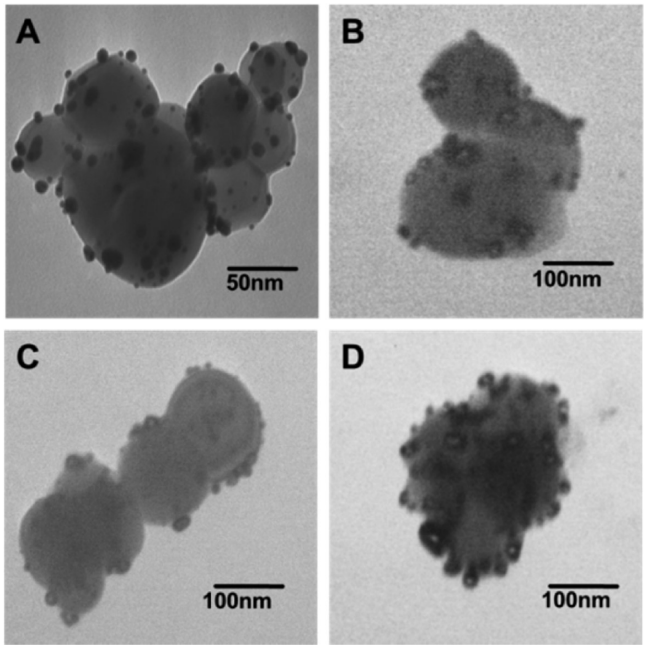

Figure 2. TEM images of (A) TiO_2–PTA–Cu, (B) TiO_2–PTA–Cu/Ag, (C) TiO_2–PTA–Cu/Pt, and (D) TiO_2–PTA–Cu/Au nanocomposites.

Electron dispersive X-ray (EDX) analysis of different nanocomposites further established the formation of respective metal alloy nanoparticles on the TiO_2–PTA surface (Figure 3).

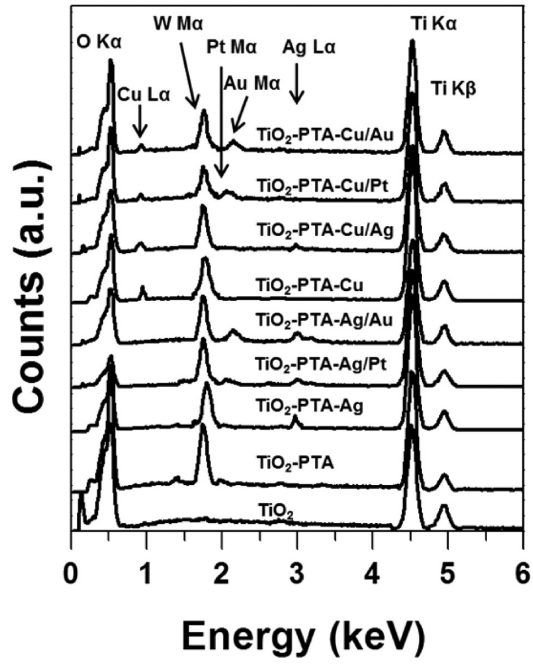

Figure 3. EDX spectra of TiO_2, TiO_2–PTA, and different TiO_2–PTA–metal composites before and after galvanic replacement.

To enable comparisons, all the EDX spectra were normalized for the intensity of the Ti Kα line. The spectrum of unmodified TiO_2 displays the peaks characteristic of Ti Kα and Kβ at 4.51 and 4.93 keV, respectively, and a peak characteristic of O Kα at 0.52 keV. TiO_2–PTA displays the peaks characteristic to Ti and O along with an additional peak attributed to the W Mα line at 1.89 keV, confirming the presence of PTA in the material.

The ability of PTA as a UV-switchable linker molecule to form TiO_2-supported TiO_2–PTA–Ag and TiO_2–PTA–Cu nanocomposites is evident from their EDX spectra that show signatures corresponding to Ag Lα at 2.98 keV and Cu Lα at 0.93 keV in the respective samples. The successful formation of bimetallic systems as a result of galvanic replacement reaction is also evident from additional peaks observed for metal species in the respective samples. For instance, TiO_2–PTA–Ag/Pt showed additional peak characteristic of Pt Mα at 2.05 keV, TiO_2–PTA–Ag/Au displayed peak characteristic of Au Mα at 2.12 keV, TiO_2–PTA–Cu/Ag showed Ag Lα signature at 2.98 keV, TiO_2–PTA–Cu/Pt showed Pt Mα energy edge at 2.05 keV, whereas TiO_2–PTA–Cu/Au showed an additional peak attributable to Au Mα at 2.12 keV.

Furthermore, UV–vis absorbance spectroscopy was employed to investigate the functionalization of TiO_2 with PTA and decoration of AgNPs and CuNPs onto TiO_2–PTA followed by galvanic replacement of these TiO_2–PTA–supported metals with different metal ions (Figure 4). TiO_2 itself shows a feature at ca. 326 nm with predominant

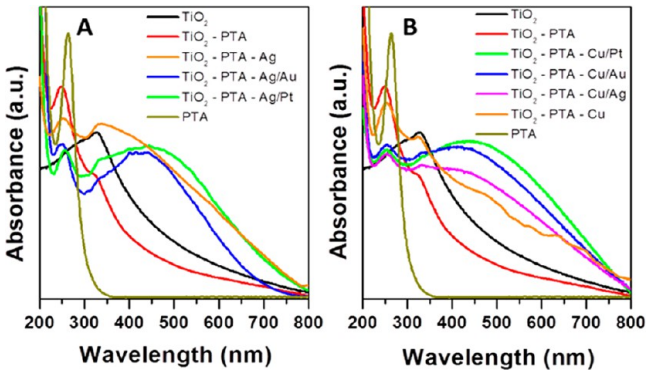

Figure 4. UV−visible spectra of (A) TiO_2−PTA−Ag nanocomposites galvanically replaced with $[AuBr_4]^-$ and $[PtCl_6]^-$ and (B) TiO_2−PTA−Cu nanocomposites galvanically replaced with Ag^+, $[AuBr_4]^-$, and $[PtCl_6]^-$.

absorbance in the UV region and a tailing feature in the visible region attributable to the scattering of the water-dispersed TiO_2 particles. Interaction between TiO_2 particles and PTA molecules results in a blue shift of characteristic PTA feature from ca. 260 to 248 nm, suggesting formation of TiO_2−PTA nanocomposite. Further decoration of TiO_2−PTA composite with AgNPs (TiO_2−PTA−Ag) results in a broad peak showing significant absorption at ca. 400−500 nm resulting from surface plasmon resonance (SPR) of AgNPs (Figure 4A). This is accompanied with a reduction and red shift in the PTA signature to 248 nm, indicating the role of PTA molecules as a linker to bind AgNPs to the TiO_2 surface. The galvanic replacement of TiO_2−PTA−Ag with $[PtCl_6]^{2-}$ and $[AuBr_4]^-$ ions results in further broadening of the SPR features in the visible region, thereby supporting the formation of TiO_2−PTA−Ag/Pt and TiO_2−PTA−Ag/Au, respectively. The galvanic replacement process for TiO_2−PTA−Cu nanocomposite with Ag^+ (TiO_2−PTA−Cu/Ag), $[PtCl_6]^{2-}$ (TiO_2−PTA−Cu/Pt), and $[AuBr_4]^-$ (TiO_2−PTA−Cu/Au) show similar trends as shown in Figure 4B whereby the weak SPR features attributable to the formation of CuNPs at ca. 500−640 nm are observed. The monometallic Cu SPR signatures broaden as a result of galvanic replacement reaction with different metal ions leading to bimetallic nanocomposite materials, which is similar to that observed in the case of Ag galvanic replacement. Notably, in our previous work,[24−26] we have demonstrated that SPR features in the visible region may be a significant contributor toward the enhancement of visible light photocatalysis, and as such, tuning of the SPR features through galvanic replacement may prove advantageous.

3.2. Surface Enhanced Raman Spectroscopy (SERS). It is well-established that metal nanoparticles can significantly enhance SERS response of an analyte molecule, wherein two cooperative mechanisms are observed to contribute in parallel to the overall SERS signal enhancement observed on a metal nanoparticle surface.[31,35,38] Among these mechanisms, the long-range electromagnetic (EM) effect contributes the most and is caused by the oscillations of surface plasmons from sub-100 nm metal features. The short-range chemical effect (CM) contributes less so than the EM effect and is associated with the chemical bonding of the probe molecule to surface defect sites such that a charge can be transferred between the molecule and the substrate. The novel TiO_2-supported bimetallic composites reported in this study exhibit both localized surface plasmon resonance from the nanosized metal particles and significant surface defect sites due to the hollow bimetallic system formed via galvanic replacement.[39,40] This renders them as potentially high quality SERS-active materials. This motivated us to investigate the SERS properties of these materials using rhodamine-6B as a probe molecule (Figure 5).

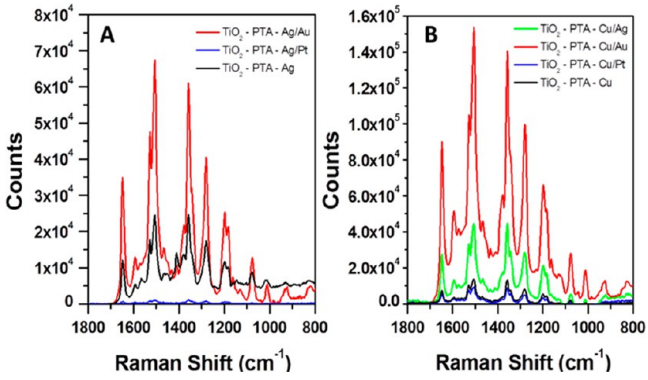

Figure 5. SERS analysis of rhodamine-6B molecules on (A) TiO_2−PTA−Ag and (B) TiO_2−PTA−Cu based nanocomposites before and after galvanic replacement with different metal ions.

Displayed in Figure 5A are the SERS spectra of rhodamine-6B molecules exposed to the TiO_2−PTA−Ag based composites, wherein we have focused on characteristic Raman signature of rhodamine-6B at ca. 1510 cm^{-1} to compare the SERS performance of different materials. Pristine TiO_2−PTA−Ag itself showed a significant SERS response (ca. 2.5×10^5 counts), which can be attributed to the high SPR absorption of AgNPs. Following galvanic replacement, TiO_2−PTA−Ag/Pt almost completely lost their SERS properties resulting in little to no signal from rhodamine-6B, while TiO_2−PTA−Ag/Au resulted in a 3.5 fold increase in the observed SERS activity and an increase in the resolution of the SERS spectra such that better resolved peaks at 1080, 920, and 820 cm^{-1} could be observed. SERS spectra of rhodamine-6B molecules exposed to the TiO_2−PTA−Cu based composites showed a similar pattern (Figure 5B). Pristine TiO_2−PTA−Cu showed less than half of SERS response in comparison to that of pristine TiO_2−PTA−Ag with 1510 cm^{-1} Raman peak counts of ca. 1.1×10^4. This difference is most likely due to well-known lower SPR cross-section of CuNPs compared to that of AgNPs. After galvanic replacement, the SERS response of TiO_2−PTA−Cu/Pt slightly reduced, while TiO_2−PTA−Cu/Ag and TiO_2−PTA−Cu/Au composites showed 4- and 15-fold increases in SERS response, respectively, over pristine TiO_2−PTA−Cu along with improved peak resolution.

3.3. Solar Light Photocatalysis. In our previous work, we demonstrated that TiO_2−PTA composites decorated with monometallic nanoparticles act as outstanding photocatalysts for degradation of organic species, wherein it was noticed that the choice of metal species plays a critical role in controlling the overall photocatalytic behavior of the system.[23−25] The novel bimetallic nanoparticles supported onto TiO_2−PTA composites prepared in this study enabled us to investigate the influence of bimetallic composition on its photocatalytic efficiency. Photoactivity of different nanocomposites was tested under simulated solar light conditions using an organic azo dye Congo red (CR) as a model analyte (Figure 6). We noticed that 8% CR molecules were degraded on exposure to solar light within 30 min in the absence of any photocatalyst. In comparison, while pristine TiO_2 particles caused ca. 26%

dx.doi.org/10.1021/am401252h | ACS Appl. Mater. Interfaces 2013, 5, 7007−7013

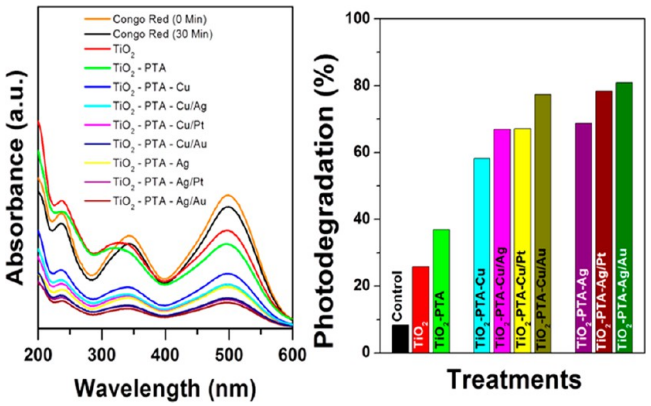

Figure 6. (A) UV−visible spectra of Congo red upon exposure to simulated solar light for 30 min in the presence of different nanocomposite photocatalysts and (B) percent photodegradation of Congo red expressed as reduction in the intensity of A_{max} at 500 nm. Control in part B represents the percent photodegradation of Congo red in the absence of a photocatalyst but in the presence of simulated solar light for 30 min.

photodegradation, TiO_2−PTA acted as a cocatalytic system resulting in ca. 37% degradation of CR. As expected, the monometallic nanocomposites, TiO_2−PTA−Cu and TiO_2−PTA−Ag enhanced the photoactivity to ca. 58% and 68%, respectively. Notably, the bimetallic systems obtained after galvanic replacement reaction showed improved photocatalytic performance over those of respective monometallic nanocomposites. For instance, both TiO_2−PTA−Cu/Pt and TiO_2−PTA−Cu/Ag were found to degrade ca. 67% of CR and TiO_2−PTA−Cu/Au was found to degrade ca. 77% of CR within 30 min of exposure to solar light. Similarly the photoactivity of TiO_2−PTA−Ag based nanocomposites enhanced to ca. 78% and 81%, respectively, after galvanic replacement of these composites with Pt and Au ions, respectively. These observations clearly show that the photococatalytic activity of TiO_2−PTA−bimetal nanocomposites can be finely tuned by the appropriate choice of bimetallic composition, wherein an increasing nobility of the metal component appears to provide a better tool for enhanced photoactivity of these materials.

4. CONCLUSIONS

This work has demonstrated a facile route for the synthesis of TiO_2-based SERS-active and photococatalytic systems decorated with bimetallic nanoparticles while employing Keggin ions of PTA as a UV-switchable localized reducing agent. The approach presented here combines the elegance of electroless galvanic replacement reaction with that of UV-switchability of PTA molecules to achieve a variety of bimetal-semiconductor nanocomposites. Investigation of the SERS and photocatalytic performance of these nanocomposites reveals that both of these properties can be controlled in a facile manner using the proposed approach. The ability to combine less expensive metals (Cu and Ag) with low quantities of highly expensive noble metals (Au and Pt) to achieve optimum outcomes for SERS and solar light photocatalysis proposes considerable promise, especially in an age where researchers are actively attempting to decrease the precious metal content in their devices.

■ ASSOCIATED CONTENT

Supporting Information

Figures S1 and S2 as mentioned in the text. This material is available free of charge via the Internet at http://pubs.acs.org.

■ AUTHOR INFORMATION

Corresponding Author

*E-mail: vipul.bansal@rmit.edu.au. Fax: +61 3 99253747. Tel.: +61 3 99252121.

Notes

The authors declare no competing financial interest.

■ ACKNOWLEDGMENTS

V.B. acknowledges the Australian Research Council (ARC) for the award of an APD Fellowship and research support through the ARC Discovery (DP0988099, DP110105125), Linkage (LP100200859), and LIEF (LE0989615, LE110100097) grant schemes. V.B. also thanks the Ian Potter Foundation for financial support towards establishing a multimode spectroscopy facility at RMIT University that was used in this study. The authors acknowledge the facilities, and the scientific and technical assistance, of the Australian Microscopy & Microanalysis Research Facility at the RMIT Microscopy & Microanalysis Facility, at RMIT University.

■ REFERENCES

(1) Satterfield, C. N. *Heterogeneous Catalysis in Industrial Practices*, Second ed.; McGraw-Hill: New York, 1991.
(2) del Arco, M.; Caballero, A.; Malet, P.; Rives, V. *J. Catal.* **1988**, 120−128.
(3) Lached, H.; Puzenat, E.; Houas, A.; Ksibi, M.; Elaloui, E.; Guillard, C.; Herrmann, J. *Appl. Catal.* **2002**, 75−90.
(4) Sharma, S. D.; Saini, K. K.; Kant, C.; Sharma, C. P.; Jain, S. C. *Appl. Catal., B* **2008**, 233−240.
(5) Barraud, E.; Bosc, F.; Edwards, D.; Keller, N.; Keller, V. *J. Catal.* **2005**, 318−326.
(6) Mahmoodi, N. M.; Arami, M.; Limaee, N. Y.; Gharanjig, K. *J. Hazard. Mater.* **2007**, 65−71.
(7) Bansal, V.; Rautaray, D.; Bharde, A.; Ahire, K.; Sanyal, A.; Ahmad, A.; Sastry, M. *J. Mater. Chem.* **2005**, *15*, 2583−2589.
(8) Hagfeldt, A.; Gratzel, M. *Acc. Chem. Res.* **2000**, 269−277.
(9) Anpo, M. *Catal. Surv. Jpn.* **1997**, 169−179.
(10) Kikuchi, H.; Kitano, M.; Takeuchi, M.; Matsuoka, M.; Anpo, M.; Kamat, P. V. *J. Phys. Chem. B* **2006**, 5537−5541.
(11) Baker, D. R.; Kamat, P. V. *Adv. Funct. Mater.* **2009**, 805−811.
(12) Bouras, P.; Stathatos, E.; Lianos, P. *Appl. Catal.* **2006**, 51−59.
(13) Wilke, K.; Breuer, H. D. *J. Photochem. Photobiol., A* **1998**, 49−53.
(14) Kudo, A.; Domen, K.; Maruya, K.; Onishi, T. *Bull. Chem. Soc. Jpn.* **1988**, 1535−1538.
(15) Heller, A.; Degani, Y.; Johnson, D. W. J.; Gallagher, P. K. *Proc. Electrochem. Soc.* **1988**, 23−33.
(16) Nosaka, Y.; Norimatsu, K.; Miyama, H. *Chem. Phys. Lett.* **1984**, *106*, 128−131.
(17) Yonezawa, T.; Matsune, H.; Kunitake, T. *Chem. Mater.* **1999**, 33−35.
(18) Colvin, V. L.; Goldstein, A. N.; Alivisatos, A. P. *J. Am. Chem. Soc.* **1992**, 5221−5230.
(19) Kamat, P. V.; Shanghavi, B. *J. Phys. Chem. B* **1997**, *101*, 7675−7679.
(20) Doron, A.; Katz, E.; Willner, I. *Langmuir* **1995**, 1313−1317.
(21) Maruyama, O.; Senda, Y.; Omi, S. *J. Non-Cryst. Solids* **1999**, 100−106.
(22) Deki, S.; Aoi, Y.; Yanagimoto, H.; Ishii, K.; Akamatsu, K.; Mizuhata, M.; Kajinami, A. *J. Mater. Chem.* **1996**, 1879−1882.
(23) Che, M.; Bennett, C. O. *Adv. Catal.* **1989**, 55−172.

(24) Pearson, A.; Jani, H.; Kalantar-zadeh, K.; Bhargava, S. K.; Bansal, V. *Langmuir* **2011**, *27*, 6661−6667.
(25) Pearson, A.; Bhargava, S. K.; Bansal, V. *Langmuir* **2011**, *27*, 9245−9252.
(26) Pearson, A.; Zheng, H.; Kalantar-zadeh, K.; Bhargava, S. K.; Bansal, V. *Langmuir* **2012**, *28*, 14470−14475.
(27) Pope, M. T.; Mueller, A. *Angew. Chem., Int. Ed.* **1991**, 34−48.
(28) Mandal, S.; Selvakannan, P.; Pasricha, R.; Sastry, M. *J. Am. Chem. Soc.* **2003**, 8440−8441.
(29) Papaconstantinou, E. *Chem. Soc. Rev.* **1989**, *18*, 1.
(30) Mandal, S.; Anandrao, B. M.; Sastry, M. *J. Mater. Chem.* **2004**, 2868−2871.
(31) Pearson, A.; O'Mullane, A. P.; Bhargava, S. K.; Bansal, V. *Electrochem. Commun.* **2012**, *25*, 87−90.
(32) Pearson, A.; O'Mullane, A. P.; Bansal, V.; Bhargava, S. K. *Chem. Commun.* **2010**, *46*, 731−733.
(33) Pearson, A.; O'Mullane, A. P.; Bansal, V.; Bhargava, S. K. *Inorg. Chem.* **2011**, *50*, 1705−1712.
(34) Pearson, A.; O'Mullane, A. P.; Bhargava, S. K.; Bansal, V. *Inorg. Chem.* **2012**, *51*, 8791−8801.
(35) Plowman, B.; Ippolito, S. J.; Bansal, V.; Sabri, Y. M.; O'Mullane, A. P.; Bhargava, S. K. *Chem. Commun.* **2009**, 5039−5041.
(36) Bansal, V.; O'Mullane, A. P.; Bhargava, S. K. *Electrochem. Commun.* **2009**, *11*, 1639−1642.
(37) Bansal, V.; Jani, H.; Du Plessis, J.; Coloe, P. J.; Bhargava, S. K. *Adv. Mater.* **2008**, *20*, 717−723.
(38) Chrimes, A. F.; Khoshmanesh, K.; Stoddart, P. R.; Kayani, A. A.; Mitchell, A.; Daima, H.; Bansal, V.; Kalantar-zadeh, K. *Anal. Chem.* **2012**, *84*, 4029−4035.
(39) Jing, C.; Fang, Y. *J. Colloid Interface Sci.* **2007**, *314*, 46−51.
(40) Jiang, J.; Bosnick, K.; Maillard, M.; Brus, L. *J. Phys. Chem. B* **2003**, *107*, 9964−9972.